Synthesis, Structure, and Spectroscopy of an Encapsulated Nickel(II) Complex of the Unsymmetrical Macrobicyclic Ligand 1-Methyl-8-amino-3,13-dithia-6,10,16,19-tetraazabicyclo[6.6.6]icosane (AMN_4S_2sar)

Therese M. Donlevy, Lawrence R. Gahan,* Robert Stranger, Sarah E. Kennedy, Karl A. Byriel, and Colin H. L. Kennard

Department of Chemistry, The University of Queensland, Brisbane 4072, Australia

Received May 11, 1993•

The nickel(II) complex of the encapsulating ligand 1-methyl-8-amino-3,13-dithia-6,10,16,19-tetraazabicyclo[6.6.6]-icosane, $[Ni(AMN_4S_2sar)]^{2+}$, is reported. Crystals of the complex are monoclinic, space group $P2_1/c$, with $Z = 4$, $a = 9.167(6)$ Å, $b = 19.885(4)$ Å, $c = 13.068(8)$ Å, $\beta = 95.37(3)°$, and $R = 0.055$. The low-temperature (~10 K) single-crystal absorption spectrum and ligand field analysis of the complex are reported. The spin-forbidden $^3A_{2g} \rightarrow {}^1E_g, {}^1A_{1g}$ transitions were observed at low temperature, and from the spectroscopic analysis, a significant differential nephelauxetic effect is shown to occur resulting in much lower values for the Racah B and C parameters for these spin-forbidden transitions in relation to the spin-allowed transitions.

Introduction

Encapsulated transition metal complexes have been studied extensively. In the majority of cases the ligands have been hexaamines of the sar type (sar = 3,6,10,13,16,19-hexaazabicyclo[6.6.6]icosane),[1-15] although metal complexes of ligands with donors other than N_6 have been reported.[16-21] As part of a study directed at the synthesis and properties of potentially octahedral encapsulating ligands with unsymmetrical nitrogen and sulfur donor sets, we have prepared the encapsulating ligands 1-methyl-8-amino-3,13-dithia-6,10,16,19-tetraazabicyclo[6.6.6]-icosane and 1-methyl-8-amino-3-thia-6,10,13,16,19-pentaazabicyclo[6.6.6]icosane based on the sarcophagine model but containing N_4S_2 and N_5S donors, respectively.[19,20] These ligands would be expected to impose unusual structural and electronic constraints on an encapsulated transition metal ion. Of interest are the electronic spectra of six-coordinate complexes of nickel(II) in these mixed-donor systems, particularly with nitrogen and thioether donors, where the lowest energy band corresponding to the $^3A_{2g} \rightarrow {}^3T_{2g}$ transition often exhibits pronounced asymmetry giving rise to a characteristic double-humped band shape. The origins of this double-humped band shape have been the object of some discussion.[22-28]

In this paper the synthesis, characterization by single-crystal X-ray analysis, and UV/vis spectroscopy of the nickel(II) complex of the ligand 1-methyl-8-amino-1,13-dithia-6,10,16,19-tetraazabicyclo[6.6.6]icosane (AMN_4S_2sar)[19] are described.

Experimental Section

Detailed synthesis and characterization of the metal-free ligand AMN_4S_2sar have been reported.[19] The magnetic susceptibility of the complex was measured by the Evans method;[29] diamagnetic corrections for the complex were calculated by using Pascal's constants.[30]

Caution! Perchlorate salts of metal complexes can be explosive and should be handled with care. They should not be heated as solids.

$[Ni(AMN_4S_2sar)](ClO_4)_2 \cdot {}^1/_2H_2O$. The ligand AMN_4S_2sar (1 g) was dissolved in methanol (10 mL). Nickel(II) perchlorate (1.16 g) dissolved in methanol (10 mL) was added slowly and the solution gently warmed. The pale pink precipitate which formed dissolved upon heating to provide a more intensely colored purple-pink solution. Crystallization was induced by permitting the solution to stand at room temperature after the addition of an aqueous solution of $NaClO_4$. Anal. Calcd for $[Ni(C_{15}H_{33}N_5S_2)](ClO_4)_2 \cdot {}^1/_2H_2O$: C, 29.3; H, 5.6; N, 11.4; S, 10.4; O, 22.2. Found: C, 29.6; H, 5.6; N, 11.1; S, 9.4; O, 21.9. Visible spectrum in H_2O [λ_{max}, nm (ϵ_{max})]: 507 (27), 333 (44). Solution magnetic moment (H_2O): 3.02 μ_B.

Visible Spectra. Visible spectra of an aqueous solution of the complex were recorded with a Hewlett Packard 8450 UV/vis spectrophotometer attached to a Hewlett Packard 7225B plotter and 8290/M flexible disk drive (ϵ in M^{-1} cm^{-1}). Electronic spectra of a single crystal of $[Ni(AMN_4S_2sar)]^{2+}$ were measured on a Cary-17 spectrophotometer which has been modified to permit control and data collection by an external computer. The original detection system of the Cary-17 has

* Author to whom correspondence should be addressed.
• Abstract published in *Advance ACS Abstracts,* November 1, 1993.

(1) Creaser, I. I.; Harrowfield, J. MacB.; Herlt, A. J.; Sargeson, A. M.; Springborg, J.; Geue, R. J.; Snow, M. R. *J. Am. Chem. Soc.* **1977**, *99*, 3181.
(2) Sargeson, A. M. *Pure Appl. Chem.* **1986**, *58*, 1511.
(3) Creaser, I. I.; Geue, R. J.; Harrowfield, J. MacB.; Herlt, A. J.; Sargeson, A. M.; Snow, M. R.; Springborg, J. *J. Am. Chem. Soc.* **1982**, *104*, 6016.
(4) Geue, R. J.; Hambley, T. W.; Harrowfield, J. MacB.; Sargeson, A. M.; Snow, M. R. *J. Am. Chem. Soc.* **1984**, *106*, 5478.
(5) Sargeson, A. M. *Chem. Br.* **1979**, *15*, 23.
(6) Bond, A. M.; Lawrance, G. A.; Lay, P. A.; Sargeson, A. M. *Inorg. Chem.* **1983**, *22*, 2010.
(7) Creaser, I. I.; Sargeson, A. M.; Zanella, A. W. *Inorg. Chem.* **1983**, *22*, 4022.
(8) Martin, L. L.; Martin, R. L.; Murray, K. S.; Sargeson, A. M. *Inorg. Chem.* **1990**, *29*, 1387.
(9) Martin, L. L.; Hagen, K. S.; Hauser, A.; Martin, R. L.; Sargeson, A. M. *J. Chem. Soc., Chem. Commun.* **1988**, 1313.
(10) Strach, S. J.; Bramley, R. *J. Chem. Phys.* **1988**, *88*, 7380.
(11) Bernhard, P.; Sargeson, A. M. *J. Chem. Soc., Chem. Commun.* **1985**, 1516.
(12) Creaser, I. I.; Harrowfield, J. MacB.; Lawrance, G. A.; Mulac, W.; Sangster, D.; Sargeson, A. M.; Schmidt, K.; Sullivan, J. C. *J. Coord. Chem.* **1991**, *23*, 389.
(13) Sotomayer, J.; Santos, H.; Pina, F. *Can. J. Chem.* **1991**, *69*, 567.
(14) Geue, R. J.; Petri, W. R.; Sargeson, A. M.; Snow, M. R. *Aust. J. Chem.* **1992**, *45*, 1681.
(15) Szcepaniak, L. S.; Sargeson, A. M.; Creaser, I. I.; Tweedle, M.; Bryant, R. G. *Bioconjugate Chem.* **1992**, *3*, 27.
(16) Gahan, L. R.; Hambley, T. W.; Sargeson, A. M.; Snow, M. R. *Inorg. Chem.* **1982**, *21*, 2699.
(17) Osvath, P.; Sargeson, A. M.; Skelton, B. W.; White, A. H. *J. Chem. Soc., Chem. Commun.* **1991**, 1036.
(18) Bernhard, P.; Bull, D. J.; Robinson, W. T.; Sargeson, A. M. *Aust. J. Chem.* **1992**, *45*, 1241.
(19) Donlevy, T. M.; Gahan, L. R.; Hambley, T. W.; Stranger, R. *Inorg. Chem.* **1992**, *31*, 4376.
(20) Bruce, J. I.; Gahan, L. R.; Hambley, T. W.; Stranger, R. *Inorg. Chem.*, submitted for publication.
(21) Osvath, P.; Sargeson, A. M. *J. Chem. Soc., Chem. Commun.* **1993**, 40.
(22) Jørgensen, C. K. *Acta Chem. Scand.* **1955**, *9*, 1362.
(23) Palmer, R. A.; Piper, T. S. *Inorg. Chem.* **1966**, *5*, 864.
(24) Dingle, R.; Palmer, R. A. *Theor. Chim. Acta* **1966**, *6*, 249.
(25) Hart, S. M.; Boeyens, J. C. A.; Hancock, R. D. *Inorg. Chem.* **1983**, *22*, 982.
(26) Gahan, L. R.; Hambley, T. W. *Transition Met. Chem.* **1988**, *13*, 72.
(27) Stranger, R.; Wallis, S. C.; Gahan, L. R.; Kennard, C. H. L.; Byriel, K. A. *J. Chem. Soc., Dalton Trans.* **1992**, 2971.
(28) Alper, J. S.; Zompa, L. J. *Inorg. Nucl. Chem.* **1980**, *42*, 1693.
(29) Evans, D. F. *J. Chem. Soc.* **1959**, 2003.
(30) Figgis, B. N.; Lewis, J. *Modern Coordination Chemistry*; Lewis, J., Wilkins, R. G., Eds.; Interscience: New York, 1960; p 403.

0020-1669/93/1332-6023$04.00/0

Table I. Crystallographic Data for $[Ni(AMN_4S_2sar)](ClO_4)_2$

cryst system	monoclinic
space group	$P2_1/c$ (No. 14)
a (Å)	9.167(6)
b (Å)	19.885(4)
c (Å)	13.068(8)
β (deg)	95.37(3)
V (Å^3)	2372(2)
D_{calc} (g/cm^{-3})	1.683
empirical formula	$C_{15}H_{33}Cl_2N_5NiO_8S_2$
fw	605.20
Z	4
μ(Mo Kα) (cm^{-1})	12.7
F(000), electrons	1248
habit	needles
dimens (mm)	0.10 × 0.12 × 0.25
temp (K)	298
radiation (λ, Å)	Mo Kα (0.710 73)
R	0.0550
R_w	0.0540
S	1.14

been replaced by a Hamamatsu R636 GaAs photomultiplier tube in the UV–visible region and a Hamamatsu P2682 thermoelectrically cooled PbS detector with a C 1103-02 temperature controller in the near-IR region. Low-temperature (~10 K) spectra were obtained using a Leybold Heraeus ROK 10–300 closed cycle helium cryostat system, for which the vacuum was $<10^{-4}$ Torr. For single-crystal spectroscopy it was necessary to cool the sample to ~250 K under atmospheric conditions prior to evacuation of the cryostat, due to significant dehydration of the crystals under vacuum. The single crystal was mounted onto a copper template with rubber cement. One edge of the crystal was not adhered to the copper template to allow for contraction and expansion upon cooling/heating of the sample. The single crystal was allowed to equilibrate for 1 h at ~10 K prior to measurement of the low-temperature spectra. Baseline spectra were recorded under identical conditions after removal of the crystal from the copper template and subtracted from the single-crystal spectra. All ligand field calculations were performed using the Fortran program CAMMAG.[31]

X-ray Crystallography. The final unit-cell parameters were obtained by least squares on the setting angles for 25 reflections between 18 and 25° (2θ), measured and refined on an Enraf-Nonius CAD4 diffractometer with a graphite monochromator. The crystallographic data are summarized in Table I. The intensities of 3 standard reflections, measured every 200 reflections throughout the data collection, showed only small random variations. The data were processed and corrected for Lorentz and polarization effects and absorption (empirical, based on azimuthal scans for 4 reflections) using the CAD-4 SDP packages.[32] It was difficult to get suitable crystals that diffracted to high 2θ. About 25% of the reflections were considered observed, and this gave a very low N_{ref}/N_{par} value of 3.5. The structure was solved by heavy-atom approach using SHELXS-86[33] and refined by block-matrix least-squares methods using SHELX 76.[34] All non-hydrogen atoms were refined with anisotropic atomic displacement parameters. Hydrogen atoms were fixed in idealized positions. Secondary extinction corrections were not applied. Neutral scattering factors and anomalous dispersion corrections for non-hydrogen atoms were taken from ref 35. The atomic nomenclature is defined in Figure 1; final atomic coordinates and equivalent isotropic thermal parameters are listed in Table II; bond lengths, bond angles, and torsion angles appear in Tables III–V, respectively. Figure 1 was drawn with PLATON.[36]

Results and Discussion

Reaction of a methanol solution of nickel(II) perchlorate with a methanol solution of the encapsulating ligand 1-methyl-8-amino-3,13-dithia-6,10,16,19-tetraazabicyclo[6.6.6]icosane (AMN_4S_2-sar) results in the formation of a purple paramagnetic (3.02 μ_B at 298 K) solid. The abbreviations employed to describe the ligand, and the complex, are those described in previous publications concerning the nomenclature of encapsulating ligands of the $N_{6-x}S_x$ (x = 1, 2, 3) type.[19]

The structure of the complex consists of the complex cation and two perchlorate anions. The molecular structure of the cation $[Ni(AMN_4S_2sar)]^{2+}$ with the numbering scheme is shown in Figure 1; final positional parameters and selected bond distances and angles are reported in Tables II–V, respectively. The Ni–N (average 2.103(12) Å) distances are similar to those reported for the hexaamine encapsulated complexes $[Ni(diAMN_6sarH_2)](NO_3)_4 \cdot H_2O$ (Ni–N_{av} = 2.109(5) Å), $[Ni(diAMN_6sarH_2)]$-

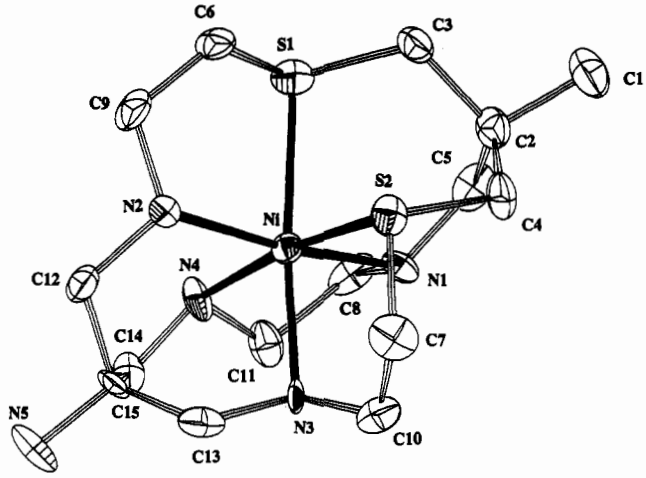

Figure 1. Numbering scheme for the cation $[Ni(AMN_4S_2sar)]^{2+}$. Hydrogen atoms have been omitted for clarity. Thermal ellipsoids are drawn to enclose 30% of the probability distribution.

Table II. Final Coordinates and Equivalent Isotropic Thermal Parameters of the Non-Hydrogen Atoms for $[Ni(AMN_4S_2sar)](ClO_4)_2$

atom	x	y	z	U(eq)[a] (Å^2)
Ni(1)	0.2298(2)	0.11876(10)	0.27037(16)	0.0316(7)
S(1)	0.3786(5)	0.1157(3)	0.1291(3)	0.0500(17)
S(2)	0.3944(5)	0.0396(2)	0.3584(3)	0.0450(17)
N(1)	0.0953(14)	0.0461(6)	0.1908(9)	0.036(5)
N(2)	0.3675(15)	0.1981(6)	0.3262(10)	0.041(5)
N(3)	0.1070(14)	0.1116(6)	0.3980(9)	0.033(5)
N(4)	0.0680(14)	0.1873(6)	0.2150(10)	0.041(5)
N(5)	0.0835(17)	0.2916(7)	0.4583(11)	0.065(7)
C(1)	0.363(2)	–0.0910(9)	0.1163(15)	0.069(8)
C(2)	0.3278(18)	–0.0241(8)	0.1688(13)	0.049(7)
C(3)	0.439(2)	0.0281(9)	0.1328(12)	0.048(7)
C(4)	0.3415(19)	–0.0347(8)	0.2853(12)	0.051(7)
C(5)	0.1691(19)	–0.0047(9)	0.1289(12)	0.050(7)
C(6)	0.5263(19)	0.1626(9)	0.1992(13)	0.051(7)
C(7)	0.307(2)	0.0351(9)	0.4747(12)	0.058(8)
C(8)	–0.0060(19)	0.0852(9)	0.1180(12)	0.049(7)
C(9)	0.464(2)	0.2204(10)	0.2486(14)	0.055(8)
C(10)	0.143(2)	0.0504(9)	0.4593(13)	0.055(8)
C(11)	–0.063(2)	0.1450(9)	0.1757(13)	0.050(7)
C(12)	0.2841(19)	0.2560(8)	0.3695(13)	0.044(7)
C(13)	0.1366(19)	0.1742(10)	0.4619(13)	0.054(8)
C(14)	0.0270(17)	0.2338(8)	0.2953(14)	0.047(7)
C(15)	0.1270(18)	0.2381(8)	0.3946(12)	0.036(6)
Cl(1)	0.7080(6)	0.3130(3)	0.0157(5)	0.061(2)
O(11)	0.7221(19)	0.2497(8)	–0.0300(14)	0.134(9)
O(12)	0.7860(19)	0.3115(8)	0.1118(12)	0.128(9)
O(13)	0.5602(15)	0.3297(8)	0.0273(11)	0.093(7)
O(14)	0.7681(18)	0.3598(9)	–0.0458(17)	0.156(10)
Cl(2)	0.1936(6)	0.4382(3)	0.2565(4)	0.055(2)
O(21)	0.2174(14)	0.4374(7)	0.3651(10)	0.071(6)
O(22)	0.2991(15)	0.3986(6)	0.2096(10)	0.074(6)
O(23)	0.2056(15)	0.5069(6)	0.2216(10)	0.081(6)
O(24)	0.0481(15)	0.4147(7)	0.2251(11)	0.086(7)

[a] U(eq) = one-third of the trace of the orthogonalized U.

(31) Cruse, D. A.; Davies, J. E.; Gerloch, M.; Harding, J. H.; Mackey, D. J.; McMeeking, R. F. CAMMAG, a Fortran Computing Package, University Chemical Laboratory, Cambridge, 1979.
(32) Enraf-Nonius Structure Determination Package, Enraf-Nonius, Delft, Holland, 1985.
(33) Sheldrick, G. M. SHELXS-86, Program for Solution of Crystal Structures, University of Gottingen, 1986.
(34) Sheldrick, G. M. SHELX 76, Program for Crystal Structure Determination, University of Cambridge, 1976.
(35) Ibers, J. A., Hamilton, W. C., Eds. *International Tables for X-ray Crystallography*; Kynoch Press: Birmingham, U.K., 1974; Vol. IV.
(36) Spek, A. L. PLATON 91, Program for Producing Drawings of Molecules, University of Utrecht, 1991.

Table III. Bond Distances (Å) for $[Ni(AMN_4S_2sar)](ClO_4)_2$

Ni(1)–S(1)	2.397(5)	N(3)–C(13)	1.51(2)
Ni(1)–S(2)	2.399(5)	N(4)–C(11)	1.52(2)
Ni(1)–N(1)	2.109(12)	N(4)–C(14)	1.47(2)
Ni(1)–N(2)	2.108(13)	N(5)–C(15)	1.43(2)
Ni(1)–N(3)	2.103(12)	C(1)–C(2)	1.54(2)
Ni(1)–N(4)	2.093(13)	C(2)–C(3)	1.56(2)
S(1)–C(3)	1.827(19)	C(2)–C(4)	1.53(2)
S(1)–C(6)	1.819(18)	C(2)–C(5)	1.55(2)
S(2)–C(4)	1.801(16)	C(6)–C(9)	1.46(3)
S(2)–C(7)	1.785(17)	C(7)–C(10)	1.53(3)
N(1)–C(5)	1.49(2)	C(8)–C(11)	1.53(2)
N(1)–C(8)	1.49(2)	C(12)–C(15)	1.55(2)
N(2)–C(9)	1.47(2)	C(13)–C(15)	1.54(2)
N(2)–C(12)	1.52(2)	C(14)–C(15)	1.52(2)
N(3)–C(10)	1.48(2)		

Table IV. Bond Angles (deg) for $[Ni(AMN_4S_2sar)](ClO_4)_2$

S(1)–Ni(1)–S(2)	88.56(17)	C(10)–N(3)–C(13)	111.1(12)
S(1)–Ni(1)–N(1)	87.2(4)	Ni(1)–N(4)–C(11)	105.6(9)
S(1)–Ni(1)–N(2)	85.4(4)	Ni(1)–N(4)–C(14)	112.5(10)
S(1)–Ni(1)–N(3)	174.2(4)	C(11)–N(4)–C(14)	110.0(12)
S(1)–Ni(1)–N(4)	100.7(4)	C(1)–C(2)–C(3)	105.7(14)
S(2)–Ni(1)–N(1)	95.7(4)	C(1)–C(2)–C(4)	108.8(14)
S(2)–Ni(1)–N(2)	89.8(4)	C(1)–C(2)–C(5)	107.1(14)
S(2)–Ni(1)–N(3)	86.2(4)	C(3)–C(2)–C(4)	113.4(13)
S(2)–Ni(1)–N(4)	170.7(4)	C(3)–C(2)–C(5)	110.7(13)
N(1)–Ni(1)–N(2)	170.7(5)	C(4)–C(2)–C(5)	110.9(13)
N(1)–Ni(1)–N(3)	90.7(5)	S(1)–C(3)–C(2)	116.0(12)
N(1)–Ni(1)–N(4)	85.0(5)	S(2)–C(4)–C(2)	114.1(11)
N(2)–Ni(1)–N(3)	97.1(5)	N(1)–C(5)–C(2)	116.4(13)
N(2)–Ni(1)–N(4)	90.8(5)	S(1)–C(6)–C(9)	108.8(13)
N(3)–Ni(1)–N(4)	84.5(5)	S(2)–C(7)–C(10)	113.1(11)
Ni(1)–S(1)–C(3)	101.3(6)	N(1)–C(8)–C(11)	108.3(13)
Ni(1)–S(1)–C(6)	92.8(6)	N(2)–C(9)–C(6)	110.6(15)
C(3)–S(1)–C(6)	105.4(8)	N(3)–C(10)–C(7)	113.7(14)
Ni(1)–S(2)–C(4)	99.1(6)	N(4)–C(11)–C(8)	107.6(14)
Ni(1)–S(2)–C(7)	97.4(6)	N(2)–C(12)–C(15)	114.5(13)
C(4)–S(2)–C(7)	106.9(8)	N(3)–C(13)–C(15)	111.5(13)
Ni(1)–N(1)–C(5)	117.2(10)	N(4)–C(14)–C(15)	118.0(13)
Ni(1)–N(1)–C(8)	105.0(9)	N(5)–C(15)–C(12)	105.5(13)
C(5)–N(1)–C(8)	107.1(11)	N(5)–C(15)–C(13)	106.6(13)
Ni(1)–N(2)–C(9)	111.4(10)	N(5)–C(15)–C(14)	111.1(13)
Ni(1)–N(2)–C(12)	113.0(10)	C(12)–C(15)–C(13)	107.8(13)
C(9)–N(2)–C(12)	112.5(13)	C(12)–C(15)–C(14)	109.3(13)
Ni(1)–N(3)–C(10)	112.1(10)	C(13)–C(15)–C(14)	116.0(14)
Ni(1)–N(3)–C(13)	107.5(9)		

$Cl_4 \cdot H_2O$ (Ni–N_{av} = 2.111(5) Å),[37-40] and $[Ni(diAZAN_6sar)]^{2+}$ (Ni–N_{av} = 2.105 Å).[41] The Ni–S distances (average 2.398(5) Å) are similar to those reported for $[Ni([9]aneS_3)_2]^{2+}$ (average 2.386(1) Å),[42] $[Ni(18S6)]^{2+}$ (average 2.387 Å),[43] and $[Ni([9]aneN_{3-x}S_x)_2]^{2+}$ (x = 1, 2.418(1) Å;[44] x = 2, 2.408(1), 2.415(1) Å [45]) and are at the short end of the range observed for the nickel(II) complex of the hexakis(thioether) ligand 1,1,1-tris(((2-(methylthio)ethyl)thio)methyl)ethane (range 2.397(2)–2.436(2) Å).[46] The trigonal twist angle Φ (average ~49°) is not well defined.

Six conformations are possible for complexes with the sar type ligands.[38] In the complex described in this work, two of the three five-membered chelate rings ($S(1)CH_2CH_2N(2)$; $N(1)CH_2CH_2N(4)$) adopt conformations with their C–C axes parallel (*lel*) with respect to the long axis; the third ring ($S(2)CH_2CH_2N(3)$) adopts the oblique (*ob*) conformation. The overall conformation of the complex is therefore described as lel_2ob. The E–$C_{chelate}$ (E = NH, S) torsion angles (Table V) are consistent with those displayed by other encapsulated complexes possessing chelate rings in these conformations.[38] The lel_2ob conformation has been found for the $[Ni(diAMN_6sarH_2)]Cl_4 \cdot H_2O$ complex, while the analogous $[Ni(diAMN_6sarH_2)](NO_3)_4 \cdot H_2O$ complex has the lel_3 conformations,[38-40] an example of the contribution of structural subtleties and environmental effects to the total strain of the possible conformers.[38]

Electronic Spectra. The electronic spectra of octahedral complexes of Ni(II) containing nitrogen and thioether donor ligands is of some interest. First, anomalous double-humped band shapes are often observed for the lowest energy $^3A_{2g} \rightarrow {}^3T_{2g}$ spin-allowed transition due to the close approach of the spin-forbidden $^3A_{2g} \rightarrow {}^1E_g$ transition, which gains intensity from mixing with the $^3T_{2g}$ state through spin–orbit coupling.[22-26] This mixing effect was examined in some detail by us in a recent investigation of the electronic spectrum of the N_6 donor complex $[Ni([9]aneN_3)_2]^{2+}$.[27] Double-humped band shapes for the $^3A_{2g} \rightarrow {}^3T_{2g}$ transition have been observed in a number of other Ni(II) complexes including $[Ni(en)_3]^{2+}$, $[Ni(bipy)_3]^{2+}$, $[Ni(daes)_2]^{2+}$, $[Ni([9]aneN_2S)_2]^{2+}$, and $[Ni(phen)_3]^{2+}$.[22-26] Second, because of the large difference in metal–ligand covalency between nitrogen and thioether donor ligands, a substantial nephelauxetic effect, resulting in reduced values for the Racah B and C electron repulsion parameters, can occur on thioether coordination. If the $^3A_{2g} \rightarrow {}^1E_g$ and $^3A_{2g} \rightarrow {}^1A_{1g}$ spin-forbidden transitions are observed, it may also be possible to detect the presence of a significant differential nephelauxetic effect (also known as differential radial expansion)[47] arising from the covalency differences between the octahedral t_{2g} and e_g d-orbitals. In this case, transitions to excited states arising from different electron configurations may require different Racah B and C electron repulsion parameters.

In the case of Ni(II) complexes, the $^3T_{2g}$ and $^3T_{1g}(F)$ excited states both derive from the $(t_{2g})^5(e_g)^3$ configuration, whereas the third spin-allowed state, $^3T_{1g}(P)$, arises from the $(t_{2g})^4(e_g)^4$ configuration. The ^1E_g and $^1A_{1g}$ spin-forbidden states, on the other hand, both result from intraconfigurational transitions corresponding to pure spin-flips within the e_g orbitals and as a result derive from the same electronic configuration as the $^3A_{2g}$ ground state, $(t_{2g})^6(e_g)^2$. The spin-allowed $^3T_{2g}$, $^3T_{1g}(F)$, and $^3T_{1g}(P)$ states therefore involve electron repulsion effects over both the t_{2g} and e_g orbitals whereas the spin-forbidden ^1E_g and $^1A_{1g}$ states only involve electron repulsion effects within the e_g orbitals. Consequently the ^1E_g and $^1A_{1g}$ states will experience greater metal–ligand covalency, requiring lower values for the Racah B and C parameters.

For octahedral d^8 complexes, the transition energies of interest can be determined from the following expressions which take account of full configuration interaction:[48]

$$E[^3T_{2g}] = 10Dq \quad (1.1)$$

$$E[^3T_{1g}(F)] = 7.5B + 15Dq - {}^1/_2(225B^2 + 100Dq^2 - 180BDq)^{1/2} \quad (1.2)$$

$$E[^3T_{1g}(P)] = 7.5B + 15Dq + {}^1/_2(225B^2 + 100Dq^2 - 180BDq)^{1/2} \quad (1.3)$$

(37) Comba, P.; Sargeson, A. M.; Engelhardt, L. M.; Harrowfield, J. MacB.; White, A. H.; Horn, E.; Snow, M. R. *Inorg. Chem.* **1985**, *24*, 2325.
(38) Comba, P. Inorg. *Chem.* **1989**, *28*, 426.
(39) Clark, I. J.; Creaser, I. I.; Engelhardt, L. M.; Harrowfield, J. MacB.; Krausz, E. R.; Moran, G. M.; Sargeson, A. M.; White, A. H. *Aust. J. Chem.* **1993**, *46*, 111.
(40) Engelhardt, L. M.; Harrowfield, J. MacB.; Sargeson, A. M.; White, A. H. *Aust. J. Chem.* **1993**, *46*, 127.
(41) Suh, M. P.; Shin, W.; Kim, D.; Kim, S. *Inorg. Chem.* **1984**, *23*, 618.
(42) Setzer, W. N.; Ogle, C. A.; Wilson, G. S.; Glass, R. G. *Inorg. Chem.* **1983**, *22*, 266.
(43) Cooper, S. R.; Rawle, S. C.; Hartmann, J. R.; Hintsa, E. J.; Admans, G. A. *Inorg. Chem.* **1988**, *27*, 1209.
(44) Hart, S. M.; Boeyens, J. C. A.; Michael, J. P.; Hancock, R. D. *J. Chem. Soc., Dalton Trans.* **1983**, 1601.
(45) McAuley, A.; Subramanian, S. *Inorg. Chem.* **1990**, *29*, 2830.
(46) Thorne, C. M.; Rawle, S. C.; Admans, G. A.; Cooper, S. R. *Inorg. Chem.* **1986**, *25*, 3850.
(47) Jørgensen, C. K. *Absorption Spectra and Chemical Bonding in Complexes*; Pergamon Press: Oxford, U.K., 1962.
(48) Expressions 1.1–1.5 were derived using an algebraic computer package (*DERIVE – A Mathematical Assistant*", Version 1.1, Soft Warehouse Inc., Honolulu, HI, 1988) and checked against calculated octahedral d^8 energies using a reliable ligand-field program.[31]

Table V. Torsion Angles (deg) for $[Ni(AMN_4S_2sar)](ClO_4)_2$

C(1)–C(2)–C(3)–S(1)	152.3(12)	C(4)–C(2)–C(3)–S(1)	−88.6(15)
C(5)–C(2)–C(3)–S(1)	36.7(17)	C(1)–C(2)–C(4)–S(2)	150.7(12)
C(3)–C(2)–C(4)–S(2)	33.4(18)	C(5)–C(2)–C(4)–S(2)	−91.8(15)
C(1)–C(2)–C(5)–N(1)	162.3(14)	C(3)–C(2)–C(5)–N(1)	−83.0(17)
C(4)–C(2)–C(5)–N(1)	43.7(19)	C(2)–C(3)–S(1)–C(6)	129.4(12)
C(2)–C(4)–S(2)–C(7)	147.1(12)	C(2)–C(5)–N(1)–C(8)	148.1(14)
C(9)–C(6)–S(1)–C(3)	−149.1(12)	S(1)–C(6)–C(9)–N(2)	64.1(16)
C(10)–C(7)–S(2)–C(4)	−74.6(14)	S(2)–C(7)–C(10)–N(3)	−47.8(17)
C(11)–C(8)–N(1)–C(5)	−170.4(13)	N(1)–C(8)–C(11)–N(4)	60.2(16)
C(6)–C(9)–N(2)–C(12)	−172.3(14)	C(7)–C(10)–N(3)–C(13)	−78.0(17)
C(8)–C(11)–N(4)–C(14)	−163.6(13)	C(15)–C(12)–N(2)–C(9)	144.7(14)
N(2)–C(12)–C(15)–N(5)	164.8(13)	N(2)–C(12)–C(15)–C(13)	51.3(17)
N(2)–C(12)–C(15)–C(14)	−75.6(16)	C(15)–C(13)–N(3)–C(10)	169.5(13)
N(3)–C(13)–C(15)–N(5)	151.7(13)	N(3)–C(13)–C(15)–C(12)	−95.4(15)
N(3)–C(13)–C(15)–C(14)	27.5(19)	C(15)–C(14)–N(4)–C(11)	132.0(14)
N(4)–C(14)–C(15)–N(5)	172.0(13)	N(4)–C(14)–C(15)–C(12)	56.0(18)
N(4)–C(14)–C(15)–C(13)	−66.1(19)		

$$E[^1E_g] = 8.5B + 2C + 10Dq - {}^1/_2(49B^2 + 400Dq^2 + 40BDq)^{1/2} \quad (1.4)$$

$$E[^1A_{1g}] = 17B + 4.5C + 10Dq - {}^1/_2(100B^2 + 25C^2 + 400Dq^2 + 100BC + 80BDq + 40CDq)^{1/2} \quad (1.5)$$

From these expressions, it is clear that the $^3A_{2g} \rightarrow {}^3T_{2g}$ spin-allowed transition depends only on the ligand-field strength $10Dq$, whereas the $^3A_{2g} \rightarrow {}^1E_g$ spin-forbidden transition indicates dependence on all three parameters. However, since the terms involving only Dq cancel and the cross-term in BDq has only a minor effect, the $^3A_{2g} \rightarrow {}^1E_g$ transition energy is approximately independent of Dq. A similar argument also applies for the $^3A_{2g} \rightarrow {}^1A_{1g}$ spin-forbidden transition, although in this case the cross-terms involving Dq are larger and therefore the dependence on Dq greater.

The approximate independence of the $^3A_{2g} \rightarrow {}^1E_g$ transition on the ligand-field strength has important implications when examining the electronic spectra of Ni(II) complexes containing nitrogen and thioether donor ligands. To a good approximation, nitrogen and thioether donor ligands exert very similar ligand-field strengths[19,45,49] but markedly different nephelauxetic effects. As a consequence, the $^3A_{2g} \rightarrow {}^3T_{2g}$ transition energy will remain approximately unchanged on replacing nitrogen donors with thioether donors, but the energy of the spin-forbidden $^3A_{2g} \rightarrow {}^1E_g$ transition will dramatically decrease. This effect is clearly evident when comparing the electronic spectra of the related complexes $[Ni([9]aneN_3)_2]^{2+}$ and $[Ni([9]aneS_3)_2]^{2+}$ containing the N_6 and S_6 coordination, respectively.[27,50] Both complexes have very similar $^3A_{2g} \rightarrow {}^3T_{2g}$ transition energies of approximately 12 500 and 12 750 cm^{-1}, respectively, but whereas the $^3A_{2g} \rightarrow {}^1E_g$ spin-forbidden transition overlaps with the $^3A_{2g} \rightarrow {}^3T_{2g}$ spin-allowed transition in $[Ni([9]aneN_3)_2]^{2+}$, it occurs to much lower energy ($\sim$8500 cm^{-1}) well separated from the $^3A_{2g} \rightarrow {}^3T_{2g}$ transition in $[Ni([9]aneS_3)_2]^{2+}$.[51]

The single-crystal spectra of $[Ni(AMN_4S_2sar)](ClO_4)_2$ at room temperature and $\sim$10 K are shown in Figure 2. The increased intensity for the room-temperature spectrum implies a vibronic intensity mechanism is operative. The broad absorption bands at approximately 12 625, 19 755, and 30 620 cm^{-1} in the low-temperature spectrum are straightforwardly assigned to the $^3A_{2g} \rightarrow {}^3T_{2g}$, $^3A_{2g} \rightarrow {}^3T_{1g}(F)$, and $^3A_{2g} \rightarrow {}^3T_{1g}(P)$ spin-allowed transitions. Weaker, sharper features are seen to the lower energy sides of the broad $^3A_{2g} \rightarrow {}^3T_{2g}$ and $^3A_{2g} \rightarrow {}^3T_{1g}(F)$ transitions at approximately 10 545 and 17 465 cm^{-1}. Both these peaks are observed to sharpen considerably on cooling to $\sim$10 K. The peak at $\sim$10 545 cm^{-1} is assigned to the $^3A_{2g} \rightarrow {}^1E_g$ spin-forbidden transition while the peak at $\sim$17 465 cm^{-1} is presumably associated with the $^3A_{2g} \rightarrow {}^1A_{1g}$ spin-forbidden transition.

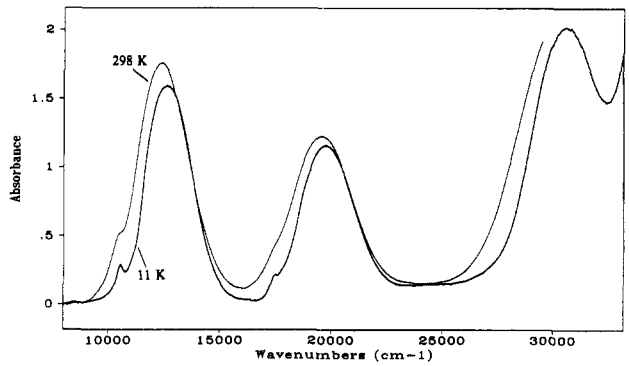

Figure 2. Single-crystal absorption spectra of $[Ni(AMN_4S_2sar)]^{2+}$ at 298 and 11 K.

The room-temperature solution spectrum of the related Ni(N_6) encapsulated complex $[Ni(diAMN_6sarH_2]^{4+}$ has recently been reported[8,39] and, typical of $Ni(N)_6$ species, the $^3A_{2g} \rightarrow {}^3T_{2g}$ band shape is double-humped due to the overlap of the $^3A_{2g} \rightarrow {}^1E_g$ spin-forbidden transition with the $^3A_{2g} \rightarrow {}^3T_{2g}$ spin-allowed transition. The lower energy component of this band at $\sim$11 390 cm^{-1} is weaker and on the basis of the spectroscopic analysis of $[Ni([9]aneN_3)_2]^{2+}$ [27] can be largely attributed to the $^3A_{2g} \rightarrow {}^1E_g$ spin-forbidden transition. The more intense band component at $\sim$12 420 cm^{-1} is therefore predominantly due to the $^3A_{2g} \rightarrow {}^3T_{2g}$ spin-allowed transition.

The position of the spin-allowed $^3A_{2g} \rightarrow {}^3T_{2g}$ transition for $[Ni(AMN_4S_2sar)]^{2+}$ reported in this study at $\sim$12 625 cm^{-1} is very close to that for $[Ni(diAMN_6sarH_2]^{4+}$, but in contrast, the spin-forbidden $^3A_{2g} \rightarrow {}^1E_g$ transition is now well resolved to lower energy indicative of a significant reduction in the Racah B and C parameters for this complex. In fact, the replacement of just two nitrogen donors with thioether ligands has led to nearly a 1000-cm^{-1} decrease in the $^3A_{2g} \rightarrow {}^1E_g$ transition energy. If one assumes an approximate linear relationship between the energy decrease of the $^3A_{2g} \rightarrow {}^1E_g$ transition and the number of thioether donors, then a $^3A_{2g} \rightarrow {}^1E_g$ transition energy of $\sim$8850 cm^{-1} is predicted for an $Ni(S_6)$ complex and this is quite close to the observed position of $\sim$8500 cm^{-1} for this transition in the complex $[Ni([9]aneS_3)_2]^{2+}$.[51] A similar linear relationship between the Racah B parameter and the number of thioether donors coordinated to the metal was recently noted by us in a series of Co(III) complexes.[19]

If the observed energies for the $^3A_{2g} \rightarrow {}^3T_{2g}, {}^3T_{1g}(F), {}^3T_{1g}(P)$ spin-allowed and $^3A_{2g} \rightarrow {}^1E_g$ spin-forbidden transitions in the low-temperature $\sim$10 K spectra of $[Ni(AMN_4S_2sar)]^{2+}$ are substituted into the expressions 1.1–1.4, the best fit ligand-field parameters are calculated to be B = 808, C = 2188, and $10Dq$ = 12 720 cm^{-1}. The observed versus calculated octahedral energies are given in Table VI. These parameter values may be compared with B = 860 and $10Dq$ = 12 420 cm^{-1} reported for $[Ni(diAMN_6sarH_2]^{4+}$,[8] though in this complex the band position

(49) Chandrasekhar, S.; McAuley, A. *J. Chem. Soc., Dalton Trans.* **1992**, 2967.
(50) Wieghardt, K.; Küppers, H.; Weiss, J. *Inorg. Chem.* **1985**, *24*, 3067.
(51) Stranger, R. Unpublished data.

Table VI. Observed and Calculated State Energies[a] (cm^{-1}) for the Low-Temperature (~10 K) Crystal Spectrum of [Ni(AMN$_4$S$_2$sar)](ClO$_4$)$_2$

		O_h calc		AOM calc
O_h state	obsd	$\zeta = 0$	$\zeta = 500$[b]	$\zeta = 0$
^1E_g	10 545	10 545	10 400 (E)	10 535
$^3T_{2g}$	12 625	12 720	12 610 (T_1)	12 505
			12 705 (E)	12 680
			12 885 (T_2)	12 750
			13 020 (A_2)	
$^1A_{1g}$	17 465	18 960	18 465 (A_1)	18 910
$^3T_{1g}$(F)	19 755	19 580	18 445 (T_1)	18 895
			19 760 (A_1)	19 660
			19 830 (T_2)	19 930
			19 895 (E)	
$^1T_{2g}$	[c]	23 005	22 995 (T_2)	22 765
				22 915
				23 110
$^1T_{1g}$	[c]	26 790	26 850 (T_1)	26 660
				26 690
				26 805
$^3T_{1g}$(P)	30 620	30 700	30 710 (E)	30 225
			30 760 (T_2)	30 395
			30 835 (T_1)	31 120
			30 860 (A_1)	

[a] Parameter values for calculations are B = 808 cm^{-1}, C = 2188 cm^{-1}, Dq = 1272 cm^{-1} (O_h calc) and e_σ(N) = e_σ(S) = 4350 cm^{-1} (AOM calc). [b] Symmetries of octahedral spin–orbit states given in parentheses. [c] Transition not observed.

for the $^3A_{2g} \rightarrow {}^3T_{2g}$ transition is not as reliable due to the overlap with the $^3A_{2g} \rightarrow {}^1E_g$ spin-forbidden transition. Even so, the value of the Racah B parameter has dropped by ~50 cm^{-1} in going from N_6 to N_4S_2 coordination.

Using the above parameter values for [Ni(AMN$_4$S$_2$sar)]$^{2+}$, the $^3A_{2g} \rightarrow {}^1A_{1g}$ spin-forbidden transition is calculated at ~18 960 cm^{-1} which falls directly beneath the broad $^3A_{2g} \rightarrow {}^3T_{1g}$(F) transition. Obviously, the weaker, sharper feature observed at ~17 465 cm^{-1} cannot be ascribed purely to the $^3A_{2g} \rightarrow {}^1A_{1g}$ spin-forbidden transition. Instead, this band is more likely the result of significant configuration interaction between the A_{1g} spin–orbit component of the $^3T_{1g}$(F) state and the spin-forbidden $^1A_{1g}$ state. In order to obtain a better fit, it is necessary to include the effects of spin–orbit coupling and possibly low-symmetry splitting. Calculations performed with the one-electron spin–orbit coupling constant ζ set to 500 cm^{-1} (see Table VI) result in better agreement between the observed and calculated energy of the spin-forbidden $^1A_{1g}$ state, but this transition is still calculated ~1000 cm^{-1} too high in energy.

Low-symmetry splitting effects can be accommodated using the angular overlap model (AOM) where the positions of the ligator atoms around the metal ion are used to generate the low-symmetry ligand-field potential. Only two AOM parameters e_σ(N) and e_σ(S) are required as the metal–thioether π interaction is generally regarded to be quite weak[52,53] and therefore is neglected in the present analysis. The differences in metal–ligand bond lengths can be accommodated by introducing a r^{-5} dependence of e_σ on bond length,[54,55] but this is not necessary in this case as all four Ni–N and both Ni–S bond lengths are equivalent once bond length uncertainties are considered (see Table III). The Racah B and C parameters used in the AOM calculations were those determined above for the octahedral calculations, while e_σ(N) and e_σ(S) were both initially set to $10Dq/3$ and then adjusted to give the best fit of the calculated energies to the observed band positions. It was found unnecessary to set e_σ(S) different from e_σ(N), and this is not unexpected as both ligands have comparable ligand-field strengths. The resulting energy levels and best fit AOM parameters are detailed in Table VI. The AOM calculations show that the low-symmetry splitting of the $^3T_{2g}$ state is small, ~250 cm^{-1}, whereas the splitting of both $^3T_{1g}$ states is much larger, around 1000 cm^{-1}. An additional calculation with ζ set to 500 cm^{-1} resulted in only a 135-cm^{-1} lower energy shift of the $^1A_{1g}$ spin-forbidden state.

Apart from the spin-forbidden $^1A_{1g}$ state, the agreement between the observed and calculated energies is very good, but the low C/B ratio of ~2.7 is unacceptable. In order to obtain some realistic estimate of this ratio, the reported band positions for the spin-allowed and spin-forbidden transitions in the low-temperature spectrum of [Ni(NH$_3$)$_6$]$^{2+}$ [56] were substituted into eq 1.1–1.5. For this complex, the $^3A_{2g} \rightarrow {}^1E_g, {}^1A_{1g}$ spin-forbidden transitions are well separated from the spin-allowed bands and therefore mixng through spin–orbit coupling can be safely ignored. Values of B = 850, C = 3440, and $10Dq$ = 11 230 cm^{-1} were obtained for [Ni(NH$_3$)$_6$]$^{2+}$ giving a C/B ratio of ~4.0, which is significantly larger than the value of 2.7 found above for [Ni(AMN$_4$S$_2$sar)]$^{2+}$. In order for the C/B ratio of ~4.0 to be considered reliable, the differential nephelauxetic effect in [Ni(NH$_3$)$_6$]$^{2+}$ must be relatively small. To show this, values of B, C, and $10Dq$ were determined separately for the spin-allowed and spin-forbidden transitions. For the spin-allowed bands, values of B = 850 and $10Dq$ = 11 230 cm^{-1} were obtained, whereas, for the spin-forbidden bands, values of B = 835 and C = 3500 cm^{-1} were found with $10Dq$ fixed at 11 230 cm^{-1}. The reduction in the Racah B value for the spin-forbidden transitions is less than 2% and, furthermore, the C/B ratio remains close to 4.

It is unlikely that the C/B ratio for [Ni(AMN$_4$S$_2$sar)]$^{2+}$ could drop as low as 2.7. Instead, the discrepancy highlights the presence of a significant differential nephelauxetic effect where lower values for the Racah B and C parameters are necessary for the $^3A_{2g} \rightarrow {}^1E_g, {}^1A_{1g}$ spin-forbidden transitions. Unfortunately, unlike [Ni(NH$_3$)$_6$]$^{2+}$, it is not possible to obtain an estimate of this effect in [Ni(AMN$_4$S$_2$sar)]$^{2+}$ by determining the values of B, C, and $10Dq$ separately for the spin-allowed and spin-forbidden transitions, as there is appreciable spin–orbit mixing between these states. However, some measure of this effect can be gained if the observed $^3A_{2g} \rightarrow {}^1A_{1g}$ transition energy is adjusted to correspond to the hypothetical transition energy in the absence of spin–orbit interaction with the $^3T_{1g}$(F) state.

The off-diagonal spin–orbit interaction between the spin-forbidden $^1A_{1g}$ state and the A_{1g} spin–orbit component of the $^3T_{1g}$(F) state is given by $\sqrt{3}\zeta$.[57] Therefore, the maximum shift of the $^1A_{1g}$ state due to this interaction is ~865 cm^{-1} for ζ = 500 cm^{-1}. If the observed $^3A_{2g} \rightarrow {}^1A_{1g}$ transition energy of 17 465 cm^{-1} is corrected for this shift, then its position in the absence of spin–orbit coupling effects is at most 18 330 cm^{-1}. Substituting this energy and the observed energy of the $^3A_{2g} \rightarrow {}^1E_g$ transition into expressions 1.5 and 1.4, respectively, with $10Dq$ held constant at 12 720 cm^{-1}, results in the values of B = 622 and C = 2874 cm^{-1}, giving a C/B ratio of ~4.6. If the C/B ratio is also constrained to ~4.2 corresponding to the value determined above for the spin-forbidden bands in [Ni(NH$_3$)$_6$]$^{2+}$, then values of B = 652 and C = 2737 cm^{-1} are calculated. In both cases a marked reduction in the Racah B parameter occurs in relation to the value of 808 cm^{-1} determined above for the spin-allowed bands in [Ni(AMN$_4$S$_2$sar)]$^{2+}$, indicating a substantial differential nephelauxetic effect in this complex.

Acknowledgment. We wish to thank Dr. T. E. Peacock for assistance with the calculations.

Supplementary Material Available: Listings of full crystal data (Table S1), hydrogen positional and thermal parameters (Table S2), (an)isotropic thermal parameters (Table S3), bond distances (Table S4), bond angles (Table S5), and torsion angles (Table S6) (7 pages). Ordering information is given on any current masthead page.

(52) Murray, S. G.; Hartley, F. R. *Chem. Rev.* **1981**, *81*, 365.
(53) Cooper, S. R. *Acc. Chem. Res.* **1988**, *21*, 141.
(54) Minomura, S.; Drickamer, H. G. *J. Chem. Phys.* **1961**, *35*, 903.
(55) Smith, D. W. *J. Chem. Phys.* **1969**, *50*, 2784.
(56) Schreiner, A. F.; Hamm, D. J. *Inorg. Chem.* **1973**, *12*, 2037.
(57) Griffith, J. S. *The Theory of Transition-Metal Ions*; Cambridge University Press: Cambridge, U.K., 1961.